Andean Geology 40 (3): 419-437. September, 2013
doi: 10.5027/andgeoV40n3-a02

Andean Geology
formerly Revista Geológica de Chile
www.andeangeology.cl

The Maipo Orocline: A first scale structural feature in the Miocene to Recent geodynamic evolution in the central Chilean Andes

César Arriagada[1], Rodolfo Ferrando[1, 3], Loreto Córdova[1, 3], Diego Morata[1], Pierrick Roperch[2]

[1] *Departamento de Geología y Centro de Excelencia en Geotermia de los Andes (FONDAP-CEGA), Universidad de Chile, Casilla 13518, Correo 21, Santiago, Chile.*
cearriag@cec.uchile.cl; dmorata@ing.uchile.cl

[2] *Géosciences Rennes, Centre National de la Recherche Scientifique (CNRS), Université de Rennes1, campus de Beaulieu, 35042, Rennes, France.*
pierrick.roperch@univ-rennes1.fr

[3] *Present address: Servicio Nacional de Geología y Minería, Avda. Santa María 0104, Santiago, Chile.*
rodolfo.ferrando@sernageomin.cl; maria.cordova@sernageomin.cl

ABSTRACT. In this paper we show the results of a paleomagnetic study carried out along the western Andes of central Chile from 30° to 36°S. Whereas paleomagnetic analysis from Jurassic to Late Cretaceous rocks in the Pampean flat slab segment shows small or non significant clockwise vertical-axis rotations, results obtained in Late Jurassic to Neogeone rocks to the south, on the normal subduction segment, show sistematically clockwise rotations up to 40º. Paleomagnetic rotations are coeval with thrusting along the High Andes in Late Miocene times. We propose a coupled Bolivian Orocline-Juan Fernández Ridge (JFR) model where a far-field component of clockwise rotation related to the formation of the Bolivian Orocline was first acquired by the margin between 31º and 33ºS. The same area was later rotated by a slight counterclockwise component related to the subduction of the JFR over the last 10 Ma. South of 33ºS the clockwise rotations related to the Bolivian Orocline component were amplified by the subduction of the JFR.

Keywords: Central Andes, Maipo Orocline, Bolivian Orocline, Juan Fernández Ridge, Paleomagnetism.

RESUMEN. El Oroclino del Maipo: Un rasgo estructural de primer orden en la evolución geodinámica Mioceno a Reciente en los Andes de Chile central. En este trabajo se muestran los resultados de un estudio paleomagnético realizado a lo largo de los Andes chilenos entre los 30º y 36ºS. Mientras que los análisis paleomagnéticos en rocas del Jurásico al Cretácico Tardío del segmento Pampeano de subducción plana muestran rotaciones de eje vertical en sentido horario pequeñas o poco significantes, los resultados obtenidos en las rocas del Jurásico Tardío al Neógeno, al sur, en el segmento de subducción normal, sistemáticamente muestran rotaciones horarias de hasta 40º. Estas rotaciones paleomagnéticas son coetáneas con cabalgamientos a lo largo de los Andes Principales durante el Mioceno Tardío. Nosotros proponemos un modelo acoplado entre el Oroclino Boliviano y el Ridge de Juan Fernández (RJF) donde una componente de campo lejano de rotación horaria relacionada con la formación del Oroclino Boliviano fue en una primera etapa adquirida por el margen entre los 31º y 33ºS. La misma región fue posteriormente rotada por una leve componente antihoraria asociada con la subducción del RJF cerca de los 10 Ma. Al sur de los 33ºS, las rotaciones horarias relacionadas con la componente del Oroclino Boliviano fueron amplificadas por la subducción del RJF.

Palabras clave: Andes centrales, Oroclino del Maipo, Oroclino Boliviano, 'Ridge' de Juan Fernández, Paleomagnetismo.

1. Introduction

The Andean margin at 33ºS (Fig. 1) is characterized by an arcuate shape, known as the Maipo Transition Zone (Yáñez *et al.,* 2002) or Maipo Orocline (Farías *et al.,* 2008). The orocline concept was originally formulated by Carey (1955) for an orogenic system which has been flexed in plan view to an elbow shape. Between 30º and 33ºS, the topography, geologic units and major structures strike N-S, whereas south of 33ºS they adopt a NNE-SSW trend (Fig. 1). While the northern segment of the curvature corresponds with the ongoing subduction of the Pampean flat slab segment which converges nearly horizontally beneath the South American lithosphere, the southern segment coincides with the normal subduction segment developed to the south of 33ºS (Isacks, 1988; Ramos *et al.,* 2002).

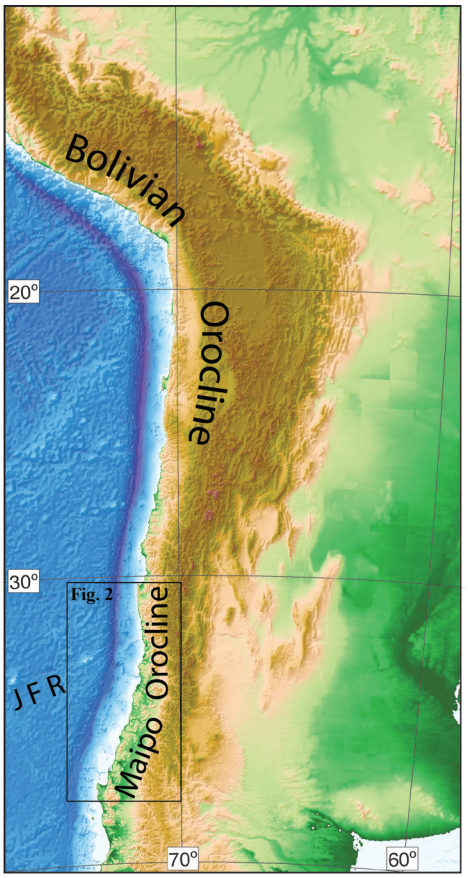

FIG. 1. Topography of the central Andes showing the Bolivian and Maipo Oroclines.

The Maipo Orocline is thought to be the result of collision of the Challenger Fracture Zone and Juan Fernández Ridge with the continent since 25 Ma (Yáñez *et al.,* 2002). The southern flank of the Maipo Orocline can be traced along strike to around 38ºS. There the Andean margin exposes another orogen bending, the Arauco Orocline (Melnick *et al.,* 2009).

Although the tectonic evolution of this segment of the Andean chain is relatively well constrained, the origin and timing of the Maipo Orocline is unclear. Paleomagnetism has proven to be very useful to characterize tectonic rotations along the western margin of the central Andes (see Arriagada *et al.,* 2008 for a recent review). In the Bolivian Orocline, along-strike variations in horizontal shortening in the back-arc provided an efficient mechanism to explain the bending of the continental margin and block rotations of the forearc region (Isacks, 1988; Arriagada *et al.,* 2008). As a first approximation, it appears reasonable that the arcuate shape of the Maipo Orocline could be accompanied by a significant pattern of rotations about a vertical axis in the forearc region and by a progressive decrease of crustal shortening and the resulting topography from north to south in the back-arc region.

Furthermore, although the Maipo Orocline is located more than 1,000 km south of the axial zone of the Central Andes, Arriagada *et al.* (2008) found that south of 30º, clockwise rotations of up to 20º could have occurred during the evolution of the Bolivian Orocline. However, evaluation of tectonic models for this segment of the Andes requires knowledge of the kinematics in this non-collisional mountain system, including detailed vertical-axis rotations of crustal blocks.

In central Chile, where few, geographically restricted, paleomagnetic studies have been carried out, knowledge about vertical-axis rotations is scarce. North of 33ºS, previous studies show no evidence for significant tectonic rotations (Beck *et al.,* 1986, 1990; Parada *et al.,* 2005; Creixell *et al.,* 2006). In contrary, south of 33ºS, both in the Coastal Cordillera and High Andes, clockwise block rotations have been observed and attributed to *in situ* block rotations in response to oblique convergence (Beck *et al.,* 1986, 1990) or to deformation of the Andean Cordillera since Early Oligocene-Middle Miocene times (Charrier *et al.,* 1996; Goguitchaichvili *et al.,* 2000). Nevertheless, near 34ºS paleomagnetic results from the

El Teniente copper-molybdenum porphyry deposit show no evidence for rotations during the last 5 Ma (Astudillo *et al.,* 2009).

In this study, we report detailed paleomagnetic results from 75 sites collected along the Coastal Cordillera and the Main Cordillera of the central Chilean Andes between 30º and 38ºS (Fig. 2) to better constrain and define the timing and origin of the Maipo Orocline.

2. Tectonic setting

The northern portion of the studied area is located in the 'Pampean flat-slab' segment (28-33°S) of the Chilean Andes, where active volcanism is absent (Barazangi and Isacks, 1976; Fig. 2). The southernmost end of the flat-slab segment changes gradationally into the 'normal-slab' segment of the southern Chilean Andes (33-46°S), characterized by a subduction angle of about 30°, where a continuous belt of modern active volcanoes occurs. Lying between the Coastal Cordillera and the High Andes in the 'normal-slab segment', the Central Depression correspond to a topographic low mostly filled by recent alluvium and pyroclastic rocks, but from where, low hills composed of mid-Cretaceous and even younger volcanic rocks emerge. This configuration of geomorphic features extends for over 500 km to the south of the area shown in figure 2.

In the Andes of central Chile, subduction has been active at least since the Late Paleozoic (Hervé *et al.,* 1988; Vergara *et al.,* 1995). Carboniferous and Jurassic plutons were emplaced in the western part of the present day Coastal Cordillera (Fig. 2), into highly deformed accretionary complexes (Hervé *et al.,* 1988; Willner *et al.,* 2000; Willner, 2005). Since the Middle Jurassic, successive magmatic arcs developed and progressively migrated eastward (Hervé *et al.,* 1988; Vergara *et al.,* 1995; Charrier *et al.,* 1996). Early to Late Cretaceous calc-alkaline plutons, bimodal volcanic sequences, clastic sedimentary rocks and limestones are exposed all along the Coastal Range forming a north-south trending belt (Vergara *et al.,* 1995). To the east, the High Andes (Fig. 2) consist of a several kilometers thick series of Jurassic to Cretaceous marine and continental back-arc sequences, as well as Cretaceous to Cenozoic continental, mainly volcanic and volcaniclastic deposits (Charrier *et al.,* 1996). Along the western flank of the High Andes, Neogene intrusive rocks are also present. An Oligocene-early Miocene magmatic arc includes the plutons that cut the western belt of the High Andes and range between 15 to 20 Ma (Kurtz *et al.,* 1997).

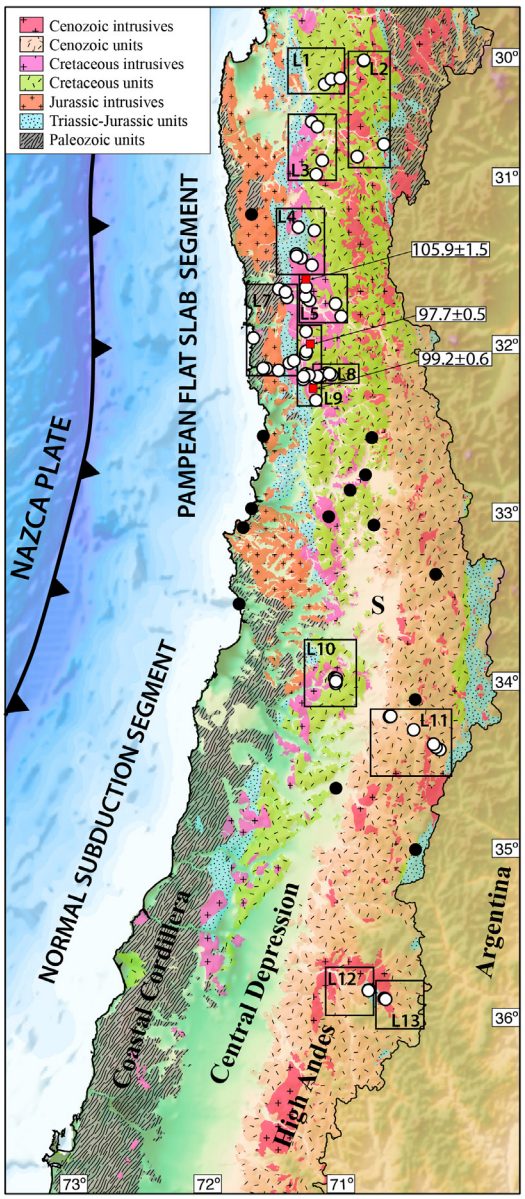

FIG. 2. Simplified geological sketch map of the Andes of central Chile and location of paleomagnetic sampling. Open circles are paleomagnetic sites from this study. Solid circles are previous paleomagnetic studies from Irwin *et al.* (1987), Creixell *et al.* (2006), Parada *et al.* (2005), Beck *et al.* (1986, 1990), Goguitchaichvili *et al.* (2000), Charrier *et al.* (1996) and Astudillo *et al.* (2009). See tables 1 and 2 for details.

TABLE 1. PALEOMAGNETIC DATA AND RESULTS.

Site	l/p/N	Dec	Inc	Dec	Inc	a95	k	Latitude °	Longitude °
Flat slab									
L3		**Illapel**	**Plutonic**	**Complex**	**100 Ma**				
04LC29	5/0/5	6.8	-50.5	-	-	2.0	1,399	-30.96977	-71.05711
04LC32	5/0/5	1.6	-60.3	-	-	8.2	88	-30.88792	-71.01247
04LC33	5/0/5	26.2	-49.4	-	-	2.1	1,296	-30.65551	-71.08195
04LC34	6/0/6	5.2	-49.6	-	-	2.7	625	-30.68752	-71.04205
mean	4	10.5	-52.8	-	-	9.8	90	-	-
L4									
08MR17	7/0/7	40.4	-64.2	-	-	3.8	259	-31.30314	-71.07583
04LC28	5/0/5	52.5	-36.0	-	-	8.3	87	-31.28151	-71.18688
08MR18	5/0/5	357.0	-55.6	-	-	8.3	86	-31.44047	-71.20478
08MR19	7/0/7	8.5	-47.1	-	-	6.5	87	-31.44047	-71.20486
04LC25	5/1/6	28.3	-45.2	-	-	6.0	138	-31.51021	-71.09740
04LC26	6/0/6	13.4	-60.3	-	-	6.7	101	-31.46470	-71.17286
04LC27	5/0/5	18.2	-55.5	-	-	5.2	214	-31.45395	-71.20220
mean	7	23.6	-53.4	-	-	11.7	28	-	-
L5									
04LC16	4/1/5	12.4	-48.7	-	-	7.7	115	-31.71880	-71.11996
04LC17	5/0/5	352.6	-58.1	-	-	5.4	204	-31.69299	-71.14552
04LC18	5/0/5	9.7	-43.9	-	-	11.3	47	-31.63706	-71.14240
04LC23	4/0/4	5.7	-59.0	-	-	5.5	279	-31.81766	-70.90108
04LC24	5/1/6	10.8	-41.8	-	-	3.1	510	-31.74172	-70.93884
mean	5	7.0	-50.5	-	-	8.8	76	-	-
L8									
09MR30	5/0/5	351.8	-46.6	-	-	4.3	324	-32.15245	-71.00982
09MR32	5/0/5	5.9	-39.7	-	-	10.4	55	-32.16698	-71.04534
09MR33	4/1/5	351.2	-61.1	-	-	3.8	470	-32.17266	-71.06090
09MR34	7/0/7	10.9	-50.1	-	-	4.0	234	-32.18100	-71.09824
10MR40	6/0/6	354.9	-55.5	-	-	1.6	1,858	-32.17279	-71.06091
10MR41	6/0/6	360.0	-58.4	-	-	3.4	396	-32.17266	-71.06091
10MR42	7/0/7	359.0	-58.8	-	-	2.7	485	-32.17266	-71.06091
10MR43	6/0/6	353.7	-62.3	-	-	3.1	474	-32.17260	-71.06084
10MR44	13/0/13	358.2	-58.2	-	-	2.0	442	-32.17270	-71.06049
10MR46	6/0/6	0.8	-57.3	-	-	2.3	828	-32.16663	-71.04364
10MR47	14/0/14	356.3	-52.2	-	-	2.5	250	-32.17197	-71.07726
10MR48	3/0/3	5.1	-55.8	-	-	5.7	467	-32.17197	-71.07725
10MR49	5/0/5	3.8	-53.8	-	-	3.9	383	-32.17197	-71.07725
mean	13	359.7	-54.8	-	-	3.7	128	-	-
L9									
08MR02	7/0/7	14.7	-54.9	-	-	7.3	70	-32.15559	-71.15690
08MR06	8/0/8	14.3	-54.5	-	-	6.2	80	-32.31282	-71.08927
09MR22	6/0/6	13.2	-55.6	-	-	13.6	25	-32.17261	-71.15760
09MR27	4/0/4	348.8	-46.1	-	-	11.5	65	-32.17128	-71.07763
04LC07	5/0/5	359.8	-58.5	-	-	9.1	72	-32.03705	-71.15495
04LC08	6/0/6	0.6	-54.5	-	-	6.5	107	-32.02039	-71.14989
04LC10	5/0/5	4.7	-59.5	-	-	5.1	223	-31.90339	-71.14928
mean	7	4.8	-55.2	-	-	5.4	126	-	-

table 1 continued.

Site	l/p/N	Dec	Inc	Dec	Inc	a95	k	Latitude °	Longitude °
Flat slab									
L7		**Jurassic**	**Intrusive**		**140-180 Ma**				
04LC01	4/3/7	220.6	50.6	-	-	4.8	186	-32.13047	-71.34668
04LC03	5/0/5	165.0	73.7	-	-	7.1	118	-32.11563	-71.43234
04LC04	6/0/6	192.8	34.4	-	-	7.8	74	-32.08920	-71.26902
04LC05	4/0/4	191.8	56.7	-	-	10.5	77	-32.07547	-71.23690
94IL01	8/0/8	25.9	-40.7	-	-	3.5	248	-31.69783	-71.27700
94IL02	13/0/13	5.4	-54.8	-	-	2.7	232	-31.64633	-71.33033
mean	6	16.9	-52.7	-	-	14.2	23	-	-
L2		**Ignimbrite (44,45)**	**Intrusive (35,37)**		**60 Ma**				
04LC44	4/0/4	3.2	-44.3	12.7	-48.6	1.6	3,387	-30.30004	-70.71906
04LC45	4/0/4	15.7	-59.7	15.7	-59.7	5.7	257	-30.29523	-70.71682
04LC35	5/0/5	355.4	-58.7	355.4	-58.7	3.0	672	-30.86811	-70.77296
04LC37	5/0/5	178.2	61.5	178.2	61.5	8.6	79	-30.79849	-70.58877
Mean IS	4	3.1	-56.3	-	-	10.5	77	-	-
Mean TC	4	-	-	6.0	-57.4	9.1	104	-	-
L6	**Sed**	**Remag**			**100 Ma**				
04LC02r	3/1/4	356.5	-54.1	326.6	-23.3	4.4	598	-32.11550	-71.45198
04LC11r	5/0/5	342.2	-58.9	352.4	-40.1	3.8	403	-31.93626	-71.51496
08M4+5	8/0/8	4.1	-55.2	-	-	6.9	66	-32.18781	-71.17399
				316.2	-52.6	17.9	11		
08MR09	5/0/5	14.8	-59.5	272.4	-21.8	3.4	515	-32.16994	-71.17118
08MR16	8/0/8	4.3	-60.2	52.6	-31.0	5.2	114	-31.66594	-71.28558
Mean IS	5	0.3	-58.0	-	-	6.5	139	-	-
Mean TC	5	-	-	333.2	-43.9	46.1	4	-	-
L1	**Sed**	**Remag**			**120 Ma**				
04LC41	14/0/14	16.7	-52.4	43.7	-53.5	2.0	404	-30.43637	-70.98824
04LC42	4/0/4	6.2	-37.0	20.5	-53.5	5.2	308	-30.40499	-70.94077
04LC43	5/0/5	17.5	-47.6	17.5	-47.6	7.2	114	-30.40198	-70.87939
Mean IS	3	12.9	-45.8	-	-	13.9	80	-	-
Mean TC	-	-	-	26.8	-52.1	14.5	74	-	-
Normal	**Subduction**	**Segment**							
L10		**Ignimbrite**			**100 Ma**				
04CM07	12/1/13	71.0	-10.6	49.6	-53.5	3.6	135	-33.96450	-70.99591
04CM08	6/0/6	65.2	-29.1	48.4	-65.8	5.6	146	-33.96568	-70.99393
04CM09	4/0/4	44.6	-40.6	345.4	-67.4	7.2	162	-33.99582	-70.98724
04CM10	7/0/7	336.7	-45.3	317.4	-42.5	4.4	192	-33.97052	-70.98300
04CM11	6/0/6	55.0	-29.8	45.8	-52.7	3.9	300	-33.98418	-70.98566
meanIS	5	48.6	-55.2	-	-	32.4	7	-	-
meanTC	5	-	-	16.7	-63.1	25.2	10	-	-

table 1 continued.

Site	l/p/N	Dec	Inc	Dec	Inc	a95	k	Latitude °	Longitude °
Flat slab									
L11		**Lava**	**Flow**		**30 Ma**				
03CM04	3/0/3	69.2	-36.2	48.2	-64.7	11.1	123	-34.19850	-70.60764
03CM05	3/0/3	238.1	32.6	195.7	34.1	5.2	424	-34.19644	-70.60054
03CM06	4/0/4	251.3	31.3	209.8	44.8	7.3	160	-34.19828	-70.59949
06CH01	7/0/7	10.7	-57.2	339.9	-35.3	5.1	141	-34.40139	-70.25119
06CH02	5/0/5	152.9	69.7	152.9	69.7	1.8	1,801	-34.38584	-70.27835
06CH03	8/0/8	334.7	-18.6	341.1	-34.2	4.0	167	-34.36695	-70.29580
06CH05	10/0/10	214.5	64.0	-	-	2.5	362	-34.28074	-70.43660
meanIS	7	34.0	-51.5	-	-	27.9	6	-	-
meanTC	7	-	-	6.4	-52.6	18.5	12	-	-
L12		**Red Beds**			**110 Ma**				
07RM01	10/3/13	318.7	-43.2	34.3	-70.1	5.1	70	-35.82116	-70.78675
07RM02	3/5/8	342.9	-37.5	12.6	-53.8	3.4	322	-35.82339	-70.79346
07RM04	6/0/6	333.2	-43.0	25.1	-64.1	5.5	148	-35.82598	-70.79443
meanIS	3	331.9	-41.7	-	-	14.9	70.0	-	-
meanTC	3	-	-	22.0	-63.0	14.7	71.0	-	-
L13		**Intrusive**			**10 Ma**				
07RM06	5/2/7	227.7	54.1	227.7	54.1	5.9	113	-35.87309	-70.67884
07RM07	7/0/7	202.7	60.5	202.7	60.5	2.7	492	-35.87309	-70.67884
07RM08	5/1/6	201.5	74.1	201.5	74.1	5.4	169	-35.87876	-70.66953
meanIS	3	213.3	63.5	-	-	19.0	43.0	-	-

l/p/N: number of lines/number of planes used in the calculation of the mean direction/N=n+l used to calculte the mean direction; **Dec**, **Inc**: mean declination and inclination *in situ* and after tilt correction; **a95**: semi-angle at 95% of confidence; **k**: Fisher's precision paramenter; **Latitude and Longitude**: site coordinate.

3. Paleomagnetic sampling and rock magnetic properties

3.1. Sampling

Paleomagnetic sampling was carried out during the course of several field seasons when we collected more than 470 oriented cores. Most of the sampling was carried out with a portable gasoline-powered drill system, and all samples were oriented *in situ* using magnetic and solar compasses.

Most samples came from intrusive rocks, but we also obtained samples from volcanic and sedimentary rocks (Table 1). In intrusive rocks, mostly from the Illapel plutonic complex, more than 80 sites were drilled with the purpose of studying pluton emplacement by determining the magnetic fabrics using the anisotropy of magnetic susceptibility (Ferrando *et al.,* in press). For these sites, there is no bedding correction but the large size of the Illapel plutonic complex suggests that it behaves as a rigid body.

Within the flat slab region sampling is more uniformly distributed than in the normal subduction segment. Because of the widespread cover of unconsolidated deposits, vegetation and the scarce road network within the normal subduction region in the High Andes, between 33º and 36ºS, most of the samples were collected along deep valleys of the Maipo, Cachapoal, Tinguiririca and Maule Rivers.

3.2. Paleomagnetic techniques and Magnetic Properties

Remanent magnetization was measured with either a spinner magnetometer (Molspin or AGICO JR5A) at the Universidad de Chile or with the 2G cryogenic magnetometer at the University of Rennes. We used

TABLE 2. TECTONIC ROTATIONS IN THE CENTRAL CHILEAN ANDES.

Locality	age	Lat(°)	Long(°)	Dobs	Iobs	a95	VGP		a95	Dexp	Iexp	R(°)	∂R	Ierr(°)	∂Ierr
L3	100	-30.970	-71.057	10.5	-52.8	9.8	87.8	29.2	11.5	2.5	-50.6	8.0	17.0	2.2	12.8
L4	100	-31.303	-71.076	23.6	-53.4	11.7	87.8	29.2	11.5	2.5	-51.0	21.1	19.3	2.4	13.7
L5	100	-31.719	-71.120	7.0	-50.5	8.8	87.8	29.2	11.5	2.6	-51.4	4.4	15.6	-0.9	12.2
L8	100	-32.152	-71.010	359.7	-54.8	3.7	87.8	29.2	11.5	2.6	-51.9	-2.9	12.1	2.9	10.3
L9	100	-32.156	-71.157	4.8	-55.2	5.4	87.8	29.2	11.5	2.6	-51.9	2.2	13.3	3.3	10.7
L7	180	-32.130	-71.347	16.9	-52.7	14.2	78.4	26.6	7.6	13.7	-52.4	3.2	20.4	0.3	13.1
L2	60	-30.300	-70.719	6.0	-57.4	9.1	82.4	168.5	4.3	352.1	-53.4	13.9	14.3	4.0	8.1
L6	100	-32.116	-71.452	0.3	-58.0	6.5	87.8	29.2	11.5	2.6	-51.9	-2.3	14.7	6.1	11.1
L1	120	-30.436	-70.988	12.9	-45.8	13.9	83.9	238.5	3.1	354.7	-44.9	18.2	16.4	0.9	11.5
L10	100	-33.965	-70.996	16.7	-63.1	25.2	87.8	29.2	11.5	2.6	-53.8	14.1	57.3	9.3	22.2
L11	30	-34.199	-70.608	6.4	-52.6	18.5	83.5	163.8	5.3	353.3	-57.2	13.1	25.8	-4.6	15.3
L12	110	-35.821	-70.787	22.0	-63.0	14.7	85.1	264.2	8.7	357.6	-50.6	24.4	28.4	12.4	14.0
L13	10	-35.873	-70.679	33.3	-63.5	19.0	85.5	139.9	3.1	357.0	-59.0	36.3	37.6	4.5	15.4
a	95	-33.000	-71.000	12.4	-55.5	1.7	86.2	178.5	6.5	355.7	-53.7	16.7	6.7	1.8	5.5
bH	100	-32.540	-70.690	10.0	-57.3	6.5	87.8	29.2	11.5	2.6	-52.3	7.4	14.6	5.0	11.1
c	100	-32.760	-70.740	5.1	-49.6	6.1	87.8	29.2	11.5	2.6	-52.5	2.5	13.4	-2.9	10.9
d	70	-33.060	-70.680	348.9	-60.9	8.3	82.3	199.0	4.8	350.8	-52.2	-1.9	14.6	8.7	7.8
e	100	-34.600	-71.000	17.0	-50.3	5.5	87.8	29.2	11.5	2.6	-54.4	14.4	13.2	-4.1	10.2
f	20	-33.610	-70.520	20.2	-54.9	6.1	82.1	131.8	4.6	356.0	-60.0	24.2	9.8	-5.1	5.8
gL	30	-34.890	-70.520	24.4	-58.4	2.4	83.5	163.8	5.3	353.3	-57.8	31.1	6.6	0.6	4.4
gH	30	-34.890	-70.520	23.2	-49.1	5.1	83.5	163.8	5.3	353.3	-57.8	29.9	8.3	-8.7	5.7
g	30	-34.890	-70.520	35.1	-44.6	3.8	83.5	163.8	5.3	353.3	-57.8	41.8	6.9	-13.2	5.0
i	5	-34.100	-70.410	2.7	-57.6	4.3	86.5	168.0	2.6	356.3	-55.3	6.4	6.9	2.3	4.0

Age: estimated age of the magnetization and of the reference pole after Besse and Courtillot (2002) used to calculate the rotation; **Lat, Long**: Latitude, longitude, position of the localities used in the calculation of the tectonic parameters; **Dobs, Iobs**: observed paleomagnetic declination and inclination; **a95**: semi-angle of confidence; **VGP**: latitude and longitude of reference poles; **Dexp, Iexp:** are the expected declination and inclination from expected pole; **R(°), ∂R, Ierr(°), ∂Ierr:** rotation and inclination error parameters and their associated errors (Demarest, 1983); localities L1-L13 from this study; locality '**a**' from Parada *et al.* (2005); locality '**Bh**' from Beck *et al.* (1990); locality '**c**' from Beck *et al.* (1990); locality '**d**' from Beck *et al.* (1986); locality '**e**' from Beck *et al.* (1986); locality '**f**' from Goguitchaichvili *et al.* (2000); locality '**g**' from Charrier *et al.* (1996); locality '**i**' from Astudillo *et al.* (2009).

both thermal cleaning and stepwise alternating field (AF) demagnetization. Demagnetization data were plotted on orthogonal diagrams (Zijderveld, 1967), and magnetization components were determined by principal component analysis (Kirschvink, 1980). For some samples and few sites (Table 1), a plane containing the characteristic direction was calculated instead of the characteristic direction. In these cases, the site-mean characteristic direction including planes and lines was calculated using the procedure described by McFadden and McElhinny (1988). Rock magnetic experiments were only performed on selected specimens from each site. We studied the acquisition of isothermal remanent magnetization (IRM) up to 1,000 mT, using an ASC pulse electromagnet. We also investigated the thermal change of the magnetic susceptibility during a heating-cooling cycle in air from room temperature to 700°C in air, using an AGICO KLY3-CS3 kappabridge instrument. Low temperature measurements were made with the MPMS XL5 cryogenic magnetometer at IPGP. We obtained well-defined characteristic directions in 57 sites from the flat slab segment and 18 sites from the normal subduction segment.

Except for sites in granite with multidomain type magnetite, most sites show stable magnetization with the principal component of magnetization going through the origin during alternating field (AF) or thermal demagnetization (TH) (Figs. 3-11). In most cases, the characteristic magnetizations correspond to a magnetization with unblocking temperatures in the range 210-560ºC. The highest unblocking temperatures (up to 680ºC) are found in oxidized ignimbrites. High unblocking temperatures are common for characteristic remanent magnetization in ignimbrites (Paquereau *et al.,* 2008). Sites in sedimentary rocks intruded by the plutonic complex have secondary magnetizations carried by pyrrhotite.

In order to discuss the tectonic implications of the paleomagnetic results and detect possible spatial variations in the amount of rotation, sites belonging to a homogeneous tectonic block were grouped into localities according to the nature and age of the magnetization. Tectonic rotation and flattening values with respect to stable South America for the individual sites were evaluated according to Demarest (1983), using reference South American paleopoles from Besse and Courtillot (2002). The site-mean directions for each locality and the tectonic rotations and inclination errors are given in Tables 1 and 2.

4. Characteristic directions

4.1. Flat Slab Domain

4.1.1. Illapel Plutonic Complex

In the flat slab domain, 'mid' Cretaceous granitic rocks and a dyke complex intruding the plutonic complex were sampled at 36 sites within the Illapel Plutonic Complex (Localities 3, 4, 5, 8 and 9 in figure 2 and Table 1). The Illapel Plutonic Complex (Parada *et al.,* 1999), early defined by Rivano *et al.* (1985) as Illapel Super Unit, intrude volcanic and volcanoclastic rocks of the Arqueros and Quebrada Marquesa formations (Fig. 2) and was subdivided into the Chalinga and Limahuida units (Rivano *et al.,* 1985). The former unit range from medium-grained gabbro to monzogranites being tonalities and granodiorites with hornblende and biotite±clinopyroxene the more abundant lithologies. Centimeter-sized mafic enclaves occur sparingly. K-Ar ages carried out on biotite and muscovite range between 113±3 Ma to 96±2 Ma (Rivano *et al.,* 1985). The second unit forms an elongated N-S band, exposed north and south of Illapel, in the central part of the Chalinga unit. Trondhjemites with plagioclase, quartz and small amounts of orthoclase, clinopyroxene and hornblende and scarce leucogranites form this unit. Three U-Pb magmatic titanite ages previously obtained by Morata *et al.* (2006) show differences in the age of crystallization between 105.9±1.5 Ma, 99.2±0.6 Ma and 97.7±05 Ma (Fig. 2).

Magnetite with unblocking temperatures below 580°C is the main magnetic carrier in most sites in intrusive rocks (Fig. 3m, n). In some sites with a trondjhemite facies, samples have low magnetic susceptibility and the characteristic magnetization is carried by a magnetic carrier with unblocking temperatures above 580°C (Fig. 3e) that is either a maghemite or a magnetite oxidized at high temperature. This magnetic phase is often observed in ignimbrites (Paquereau *et al.,* 2008). Titanomaghemite was also observed in samples from epidotized dykes and intrusives (Fig. 3a, g). K-T plots confirm the presence of maghemite in dykes belonging to the Illapel Plutonic Complex (Fig. 3l).

Both AF and thermal demagnetization were successful in isolating a stable univectorial normal polarity remanent magnetization (Fig. 3). All samples with low unblocking temperature were discarded in order to avoid a possible contamination with viscous

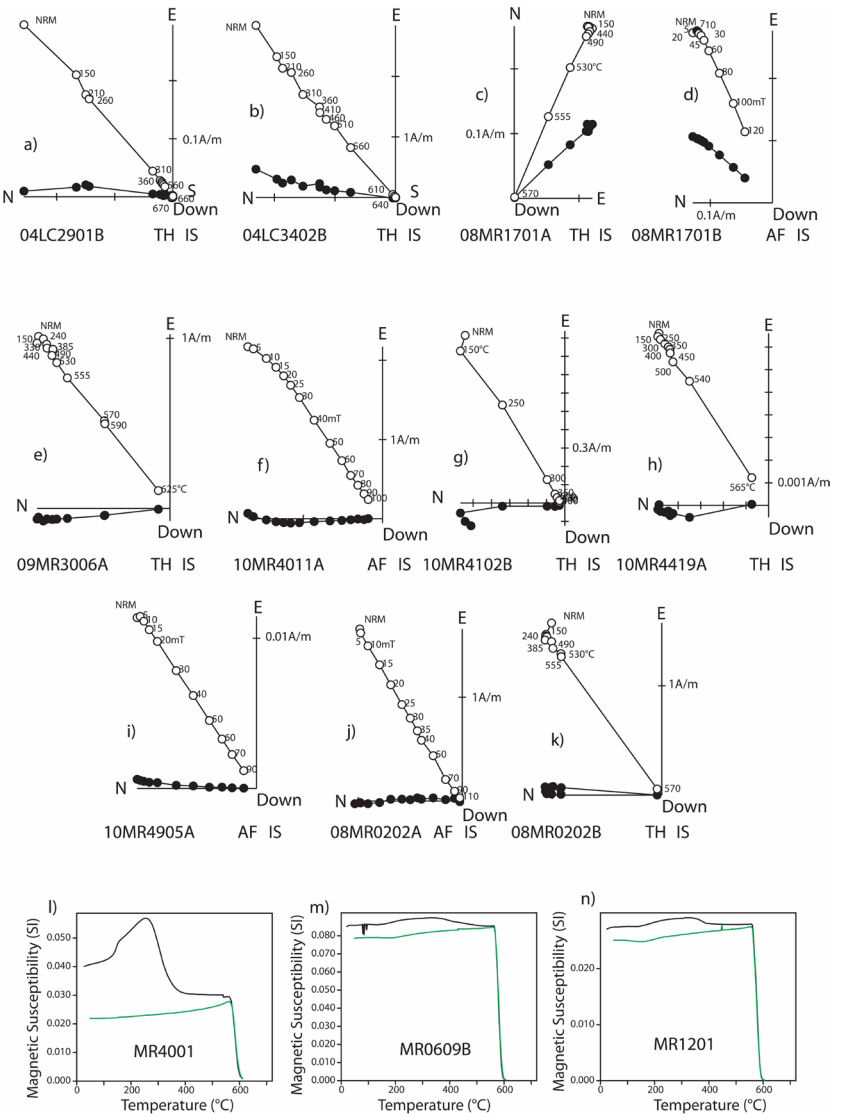

FIG. 3. **a-k.** Orthogonal AF or thermal demagnetization plots for representative samples with primary magnetizations for sites within the Illapel Plutonic Complex. Open circles correspond to the projection onto the vertical plane while filled circles correspond to projection onto the horizontal plane; **l-n.** Representative K-T plots of the Illapel Plutonic Complex.

magnetization. Only sites with high unblocking temperatures were kept for tectonic purpose. The characteristic remanent magnetization was recovered by thermal demagnetization in the temperature range 210-640ºC, or in the range 10-120 mT (Fig. 3). The presence of the normal polarity characteristic magnetization in the Illapel Plutonic Complex (Fig. 4) indicates magnetization during the Cretaceous normal polarity superchron in agreement with the age of the Illapel Plutonic Complex.

4.1.2. Jurassic Intrusives

West of the 'mid' Cretaceous Illapel Plutonic Complex (Fig. 2), a small proportion of the Coastal Cordillera is composed of a bimodal association of leucogranites, granite porphyries and gabbros of Early Jurassic age (Vergara *et al.,* 1995). Six sites were collected in the Jurassic intrusive rocks (Locality 7 in figure 2 and Table 1). Unblocking temperatures, high susceptibility values and IRM acquisition (Fig. 5) indicate that magnetite is the

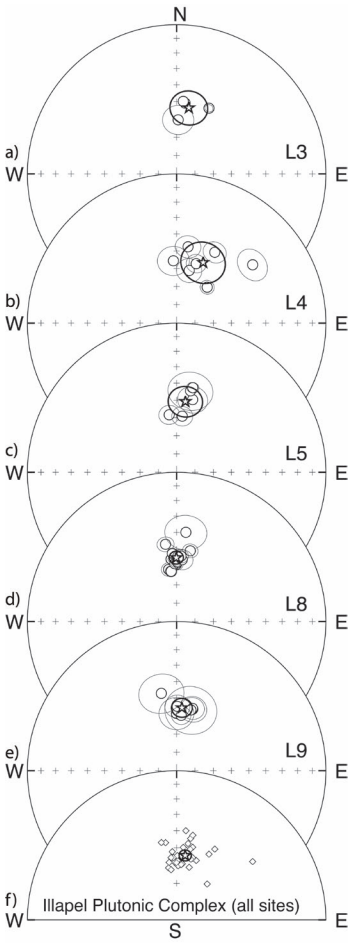

FIG. 4. **a-e.** Equal-area stereonets of characteristic directions determined along the 'mid' Cretaceous Illapel Plutonic Complex. The stars with the 95% error angle of confidence indicate the mean directions; **f.** Equal-area projection of the demagnetization data for all samples and the mean observed direction of the Illapel Plutonic Complex. Open (filled) symbols correspond to projection onto the upper (lower) hemisphere.

dominant magnetic carrier of these rocks. In contrast to Cretaceous intrusives, in this case the sites record both normal and reverse polarities.

4.1.3. Paleocene Volcanics and Intrusives

In the northern part of the study area we obtained four sites in Paleocene ignimbrites and intrusives (Locality 2 in figure 2 and Table 1). Volcanic succession consists of andesitic lavas, ignimbrites and tuffs, while intrusive bodies are of dioritic to granitic composition (Pineda and Emparan, 2006). Interpretation of the demagnetization diagrams is straightforward (Fig. 6). Unblocking temperatures and IRM acquisition (Fig. 6d) indicate that magnetite is the dominant magnetic carrier of these rocks although unblocking temperatures above 600ºC indicate that hematite also carries the same magnetization. Sites record both reverse and normal polarities. The dispersion decreases slightly after tilt correction, the kappa value of the site mean direction before the tectonic correction is 77 and after tectonic tilt correction is 104.

4.1.4. Remagnetization in sedimentary rocks

Marine and continental sedimentation associated with crustal extension occurred between the Late Triassic and Early Cretaceous all along the Coastal Range (Vergara *et al.,* 1995). Between 30º and 33ºS, clastic sedimentary rocks and limestones are exposed within the Coastal Range. These successions are tilted and also intruded by granitoids (Fig. 2). We collected samples from Triassic and Jurassic-Lower Cretaceous limestones and red sandstones close to intrusive rocks belonging to the Illapel Plutonic Complex (Localities 1 and 6 of figure 2 and Table 1). During thermal demagnetization most samples from locality 1 have characteristic magnetizations with a narrow unblocking temperature range below 300ºC (Fig. 7). Alternating field demagnetization up to 15 mT was efficient in removing the characteristic magnetization. An important decrease in the magnetic susceptibility is observed around 325ºC (Fig. 7g). The characteristic low temperature transition observed in zero field (ZFC) and field cooling (FC) of an SIRM given at 10°K is consistent with the Curie temperature of 325°C indicating pyrrhotite as the main magnetic carrier. The low medium destructive field of the magnetization at site MR09 (Fig. 7a) is due to multidomain pyrrhotite. The magnetization at sites MR05 and MR16 is also carried by pyrrhotite (Fig. 7c, d) while magnetite is also observed at sites LC02 and LC11 (Fig. 7e, f). The characteristic directions are well grouped in *in situ* coordinates and show a significant dispersion upon tilt correction (Fig. 7j, k). The paleomagnetic direction with a normal magnetic polarity is statistically indistinguishable from the mean direction of the nearby plutons of the Illapell Plutonic Complex in agreement with a remagnetization during the Cretaceous long normal polarity interval.

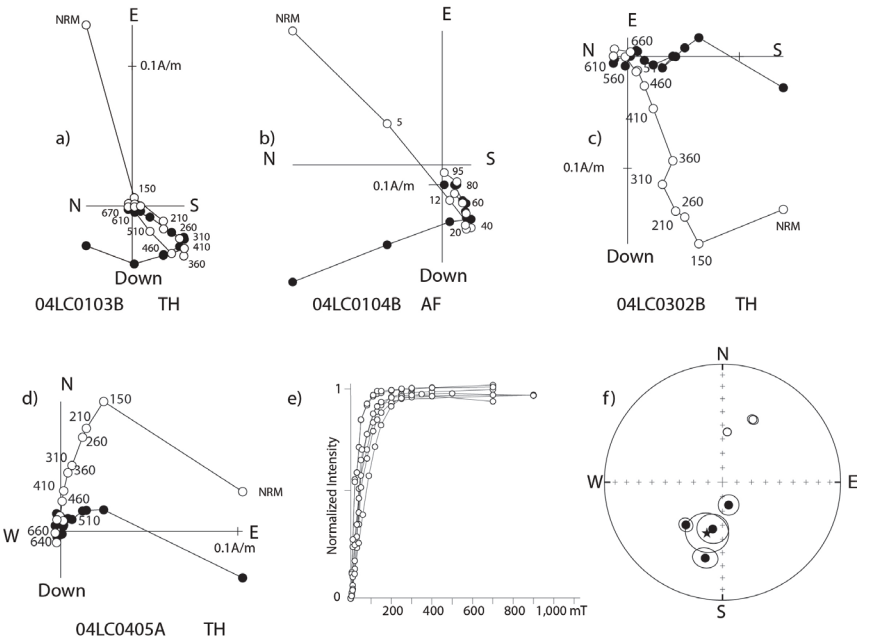

FIG. 5. **a-d.** Orthogonal AF or thermal demagnetization plots for representative samples with primary magnetizations for sites in Jurassic intrusive rocks; **e.** Normalized isothermal remanent magnetizations (IRM) for five samples of Jurassic intrusive rocks; **f.** Equal-area projection of site-mean characteristic directions in Jurassic intrusives. Same convention as in figure 3 for the orthogonal plots. For the equal-area plots, same convention as in figure 4.

To the north of the Illapel Plutonic Complex three sites were drilled in Lower Cretaceous red beds (Locality 1 in figure 2, Table 1). Secondary magnetization of normal polarity between 310 and 640ºC was found at all three sites at this locality (Fig. 8a, f). Dispersion decreases slightly in *in situ* coordinates suggesting a remagnetization. Rock-magnetic experiments (Fig. 8g) indicate that magnetite and hematite are the dominant magnetic carriers of these rocks. The dispersion slightly decreases in *in situ* coordinates (Fig. 8h, Table 1). The kappa value of the site mean direction before the tectonic correction is 80 and after tectonic tilt correction is 74.

4.2. Normal Subduction Domain

Even though several sites were collected (Table 1), we obtained stable magnetizations in only 18 sites distributed within the normal subduction segment.

4.2.1. Upper Cretaceous Ignimbrites

Upper Cretaceous silicic pyroclastic flows, andesites and volcano sedimentary breccias are exposed along the eastern flank of the Coastal Cordillera at ~34ºS (Fig. 2; Vergara *et al.,* 1995). A characteristic remanent magnetization was observed in five sites sampled from Upper Cretaceous ignimbrites (Fig. 9) (Locality 10 in Table 1 and figure 2). Even though secular variation was not fully averaged, a decrease in scatter upon tilt correction suggests a pre-folding origin for the magnetization (Fig. 9e). The kappa value of the site mean direction before the tectonic correction is 7 and after tectonic tilt correction is 10 (Table 1).

4.2.2. Oligocene Volcanics

Cenozoic continental mainly volcanic and volcanoclastic deposits are exposed along the High Andes. At locality 11, seven sites in Oligocene lava flows from the Coya-Machalí Formation (Charrier *et al.,* 1996) were collected in the Main Cordillera along the El Cobre road and the Cachapoal River valley (03CM04-06, 06CH01-05). Magnetization goes through the origin during thermal or AF demagnetization and both normal and reverse polarities were found at this locality (Fig. 10a-f). Secular variation is important at these sites and a decrease in scatter upon tilt correction suggests a primary origin for the magnetization (Fig. 10g).

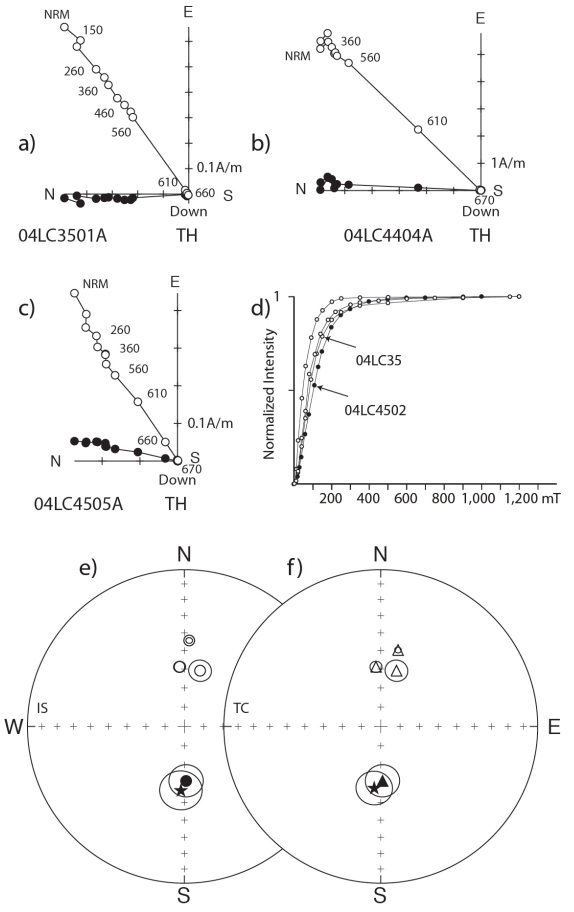

FIG. 6. **a-c.** Orthogonal thermal demagnetization plots for selected samples with primary magnetizations of Paleocene ignimbrites and intrusives; **d.** Normalized isothermal remanent magnetizations (IRM); **e** *(in situ)*-**f** *(in tilt-corrected coordinates)*. Equal-area projection of site-mean characteristic directions in Paleocene rocks. Same convention as in figure 3 for the orthogonal plots. For the equal-area plots, same convention as in figure 4.

4.2.3. Lower Cretaceous Sedimentary Rocks

Along the Maule River valley Cretaceous red sandstones were sampled at three sites (Locality 12 in Table 1 and figure 2). A primary magnetization is recorded in the temperature range 560ºC-680ºC (Fig. 11a-c).

4.2.4. Miocene Intrusives

Also in the high Maule River valley we collected three sites in Miocene intrusive rocks (Locality 13 in Table 1 and figure 2). A primary remanent magnetization of reverse polarity is recorded in the temperature range 260ºC-640ºC or with alternating fields of 10-50 mT. The normal polarity directions in after tilt correction from locality 12 are antipodal with those of reverse polarity found at locality 13 (Fig. 11e, j).

5. Tectonic rotations

For each site, tectonic rotations and inclination anomalies were calculated according to Demarest *et al.* (1983) using the reference poles after Besse and Courtillot (2002). We also included previous paleomagnetic results (Table 2, Fig. 12). Localities a-d are sites from previous studies carried out by Beck *et al.* (1986, 1990) and Parada *et al.* (2005) in Upper Cretaceous-Paleocene rocks. Except for the slight rotation (16.7±6.7) observed by Parada *et al.* (2005) localities b-d show no evidence for significant rotation. Locality f is from the results obtained by Goguitchaichvili *et al.* (2000), whereas locality e corresponds to the previous results obtained by Beck *et al.* (1986). Locality g includes the sites collected by Charrier *et al.* (1996) and locality i corresponds to the paleomagnetic results obtained by Astudillo *et al.* (2009) in the El Teniente porphyry copper deposit. No evidence for post 5 Ma rotation has been found in this locality.

We did not include the previous studies carried out by Irwin *et al.* (1987) and Creixell *et al.* (2006) in Middle Jurassic and Lower Cretaceous dike swarms and granitoid country rocks from the Coastal Cordillera. The ChRM obtained by Irwin *et al.* (1987) at all sites but one were only determined by Fisher statistics at one level of AF demagnetization and not by principal component analysis of thermal demagnetization data. Creixell *et al.* (2006) found two components of magnetization in the Jurasic dikes near Concón during detailed thermal demagnetization. AMS data and low inclinations of the primary magnetization suggested an undetected tilt of the Jurassic intrusive complex along the coast. A secondary magnetization of normal polarity was attributed to exhumation during the Cretaceous.

Available data indicate that between 30º to 31.5ºS rotations range from 8º to nearly 21º clockwise (Fig. 12, Table 2, Localities 1 to 4) affecting Cretaceous and Paleogene units. No major rotations are observed at localities 5 to 9 around 32ºS (Table 2, Fig. 12). Rotations are in general

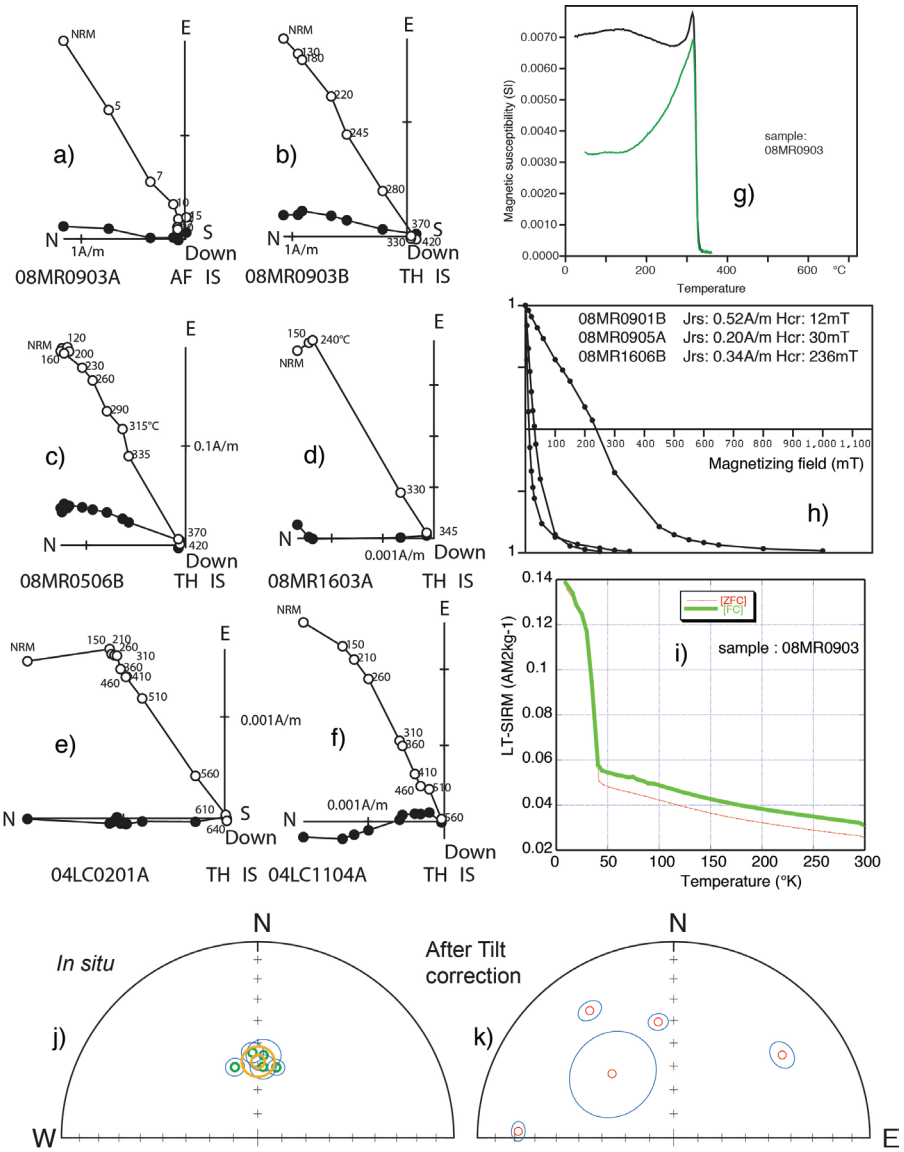

FIG. 7. Orthogonal plots of demagnetization data for five sites in sediments remagnetized by the Illapel Plutonic Complex. **a-f.** Orthogonal plots (same convention as in figure 3); **g.** thermomagnetic experiments in low field with the Agico kappabridge KLY3 susceptibilimeter and CS3 furnace. The green curve corresponds to the cooling curve; **h.** Backfield IRM acquisition; **i.** Low temperature variation of SIRM measured with the MPMS system; **j-k.** Equal-area stereonets of characteristic directions *in situ* and after tilt correction, same convention as in figure 4.

insignificant between 32º and 33ºS, but previous results show some dispersion between neighboring areas at localities a-d (Fig. 12).

Within the Pampean flat slab segment a mean rotation was calculated in three different segments, which seems to show some differences in the magnitude of rotations (Fig. 12). North of 31.5ºS the mean rotation is 15.3±5.7º (Locality 1 to 4), between 31.5º and 32.5ºS the mean rotation is 0.9±3.3º (Locality 5 to 9) while between 32.5º and 33ºS the mean rotation is 12.3±3.8º (Locality a to d). The mean rotation for all localities, including those previously published within the Pampean flat slab segment south of 30ºS listed in Table 2 is 6.9±8.1º.

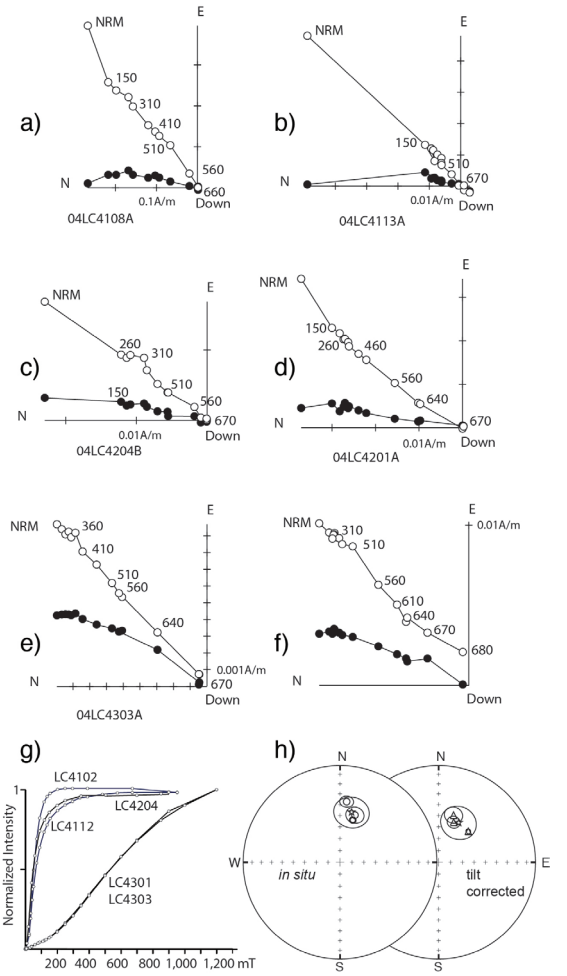

FIG. 8. **a-f.** Orthogonal plots of demagnetization data for three sites in Cretaceous remagnetized sediments; **g.** Normalized isothermal remanent magnetizations (IRM); **h.** Equal-area projection of site-mean characteristic directions. Same convention as in figure 3 for the orthogonal plots. For the equal-area plots, same convention as in figure 4.

South of 33ºS, a major change in the magnitude of rotation occurs, rotations increase and range between 13º and 42º clockwise. Rotations occur both in Mesozoic rocks of the Coastal Cordillera (Fig. 12, Locality 10 and e) and Tertiary rocks of the Main Cordillera (Fig. 12, Locality f, g, 11 and 13). The paleomagnetic rotations obtained in the Tertiary red beds and lava flows of the Abanico and Farellones Formations constrain the maximum possible age for the occurrence of rotation to the Oligocene-Early Miocene (Fig. 12, Localities 11 and 13). Results obtained by Astudillo *et al.* (2009; Locality i) show that no rotations occurred since 5 Ma. The mean rotation for all localities, between 33º and 36ºS, including those of the Coastal Cordillera (Locality 10 and e, Fig. 12) and of the High Andes (Locality f, gH and 11-13) is 24.8±10.7º.

6. Discussion

The spatial variation in the magnitude of rotations shows that the Chilean Andes region between 30º and 37ºS (Fig. 12) did not behave as a rigid block. In plan view, rotations seem to be correlated to the overall orientation of the margin. The lack of

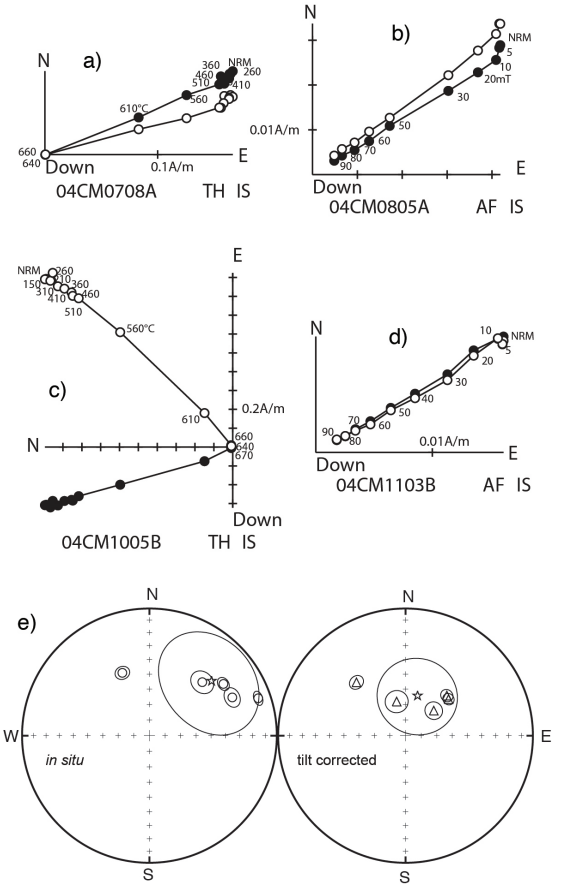

FIG. 9. **a-d.** Orthogonal AF or thermal demagnetization for representative samples with primary magnetizations of normal polarity obtained in Upper Cretaceous ignimbrites from the Coastal Cordillera; **e-f.** Equal-area projection of site-mean characteristic directions. Same convention as in figure 3 for the orthogonal plots. For the equal-area plots, same convention as in figure 4.

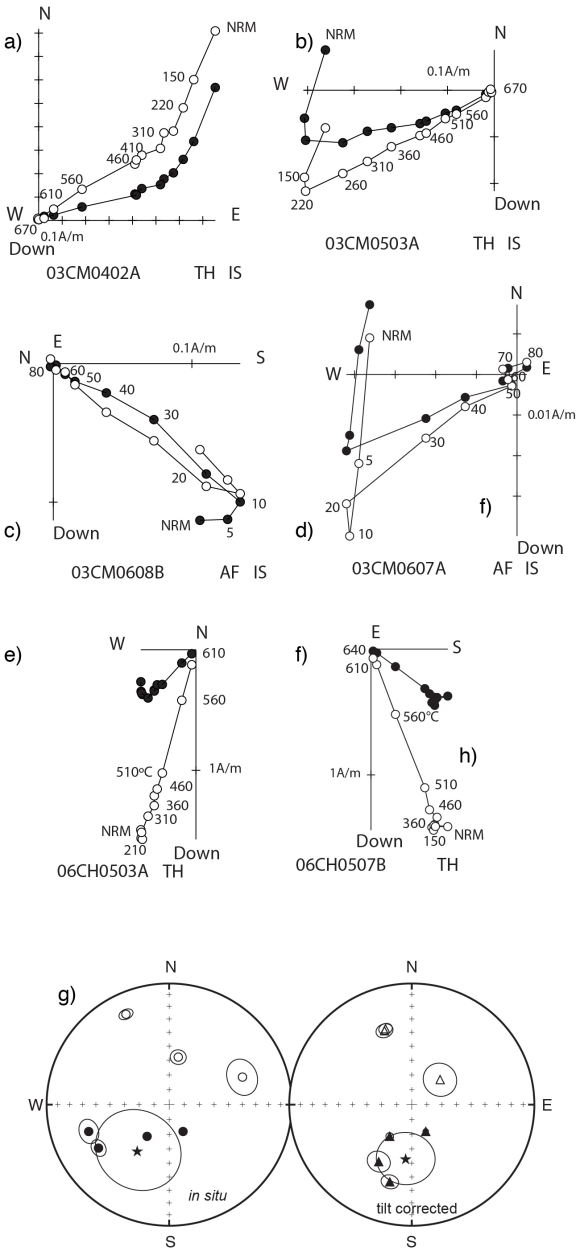

FIG. 10. **a-f.** Orthogonal AF or thermal demagnetization for representative samples with primary magnetizations obtained in Oligocene volcanic rocks from the High Andes; **g-h.** Equal-area projection of site-mean characteristic directions. Same convention as in figure 3 for the orthogonal plots. For the equal-area plots, same convention as in figure 4.

evident rotation in the northern block suggests some other coupled mechanism, for instance a larger EW coupling in the flat-slab segment.

However, another complementary mechanism would be the presence of the Juan Fernández Ridge which constitutes a discontinuous array of volcanic centers aligned roughly E-W. The origin of this aseismic ridge has been attributed to a hot spot located to the west of Alejandro Selkirk Island along the Juan Fernández Ridge. The free air gravity response of the aseismic ridge shows a continuous positive anomaly flanked by a broader negative anomaly on each side, as a result of the flexural loading of the oceanic crust. The eastward projection of the aseismic ridge roughly coincides with the Maipo Orocline (Figs. 1 and 13). Moreover, the northern edge of the Central Depression is also coincident with this continental bending and tectonic boundary (Figs. 1 and 2). The trench morphology (Fig. 1) evolves from a narrow and almost empty trench north of ~33ºS to a relatively wide turbidite-filled trench southward.

Between 18º and 30ºS, the intersection of the Juan Fernández Ridge and the subduction zone (Fig. 13) moved fairly quickly to the south between 22 and 10 Ma (Yáñez *et al.,* 2002; Le Roux *et al.,* 2005). Since 10 Ma the JFR intersection has remained relatively stable at around 33ºS (Fig. 13). In this scenario about 10º of clockwise rotation associated with the formation of the Arica deflexion would have been increased by about 10º within the normal subduction segment between 33º and 37ºS, while between 30º and 33ºS about 7º to 10º of counterclockwise rotation could explain the current pattern of no rotations in this segment. Observed paleomagnetic data are consistent with a greater shortening around 33ºS, which decreases steadily to its lowest value near 37ºS. According to estimates of shortening, from 130 to 150 km occurs in the center of the orocline while no more than 40 km of shortening occurs in its southern termination.

Arriagada *et al.* (2008) proposed a restoration of the Central Andes taking into account the paleomagnetic rotations and estimations of Andean shortening. The paleomagnetic data indicate that deformation is important prior to 20 Ma. As already shown by Martinod *et al.* (2010), the Juan Fernández Ridge entered into subduction in the Late Eocene-Oligocene near the Arica

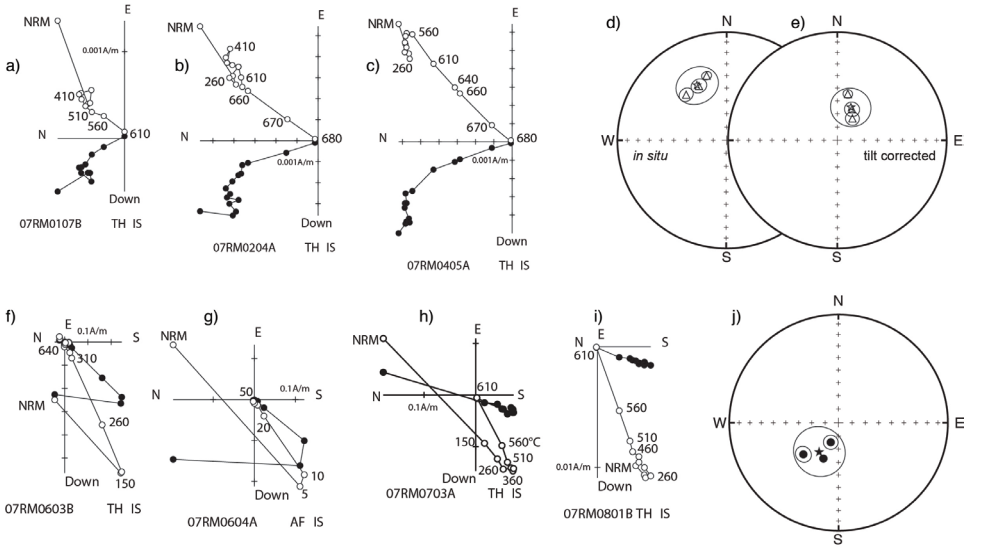

FIG. 11. **a-d.** Orthogonal thermal demagnetization plots for samples with primary magnetizations and equal-area projection (**d-e**) of site-mean characteristic directions obtained in Cretaceous red beds; **f-i.** Orthogonal AF or thermal demagnetization for samples with primary magnetizations and equal-area projection (**j**) of site-mean characteristic directions obtained in Miocene intrusive rocks. Same convention as in figure 3 for the orthogonal plots. For the equal-area plots, same convention as in figure 4.

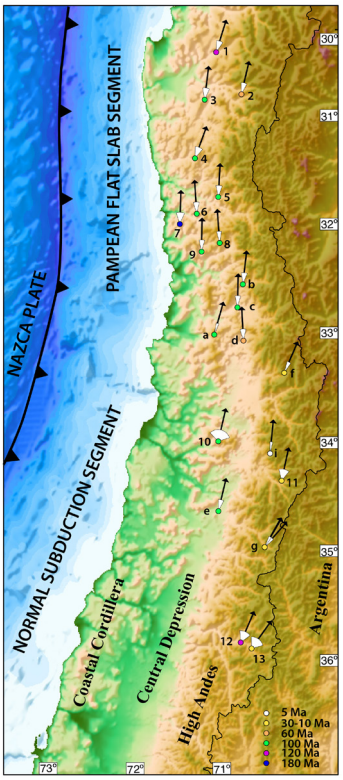

FIG. 12. Compilation of tectonic rotations (deviation of arrows from a NS direction) with errors between 30º and 37ºS. Colored circles show the inferred age of magnetization.

bend. In the reconstruction of figure 13, we use the same absolute plate rotations proposed by Yáñez *et al.* (2001) derived from a study of Gordon and Jurdy (1986). Using another hotspot reference frame changes the history of ridge subduction only changes slightly. In contrast with Yáñez *et al.* (2001), however, we attempt to take into account also the shortening and changes in shape of the margin due to Andean deformation.

While Arriagada *et al.* (2008) estimated that deformation started in central Chile at the same time as in the central Andes, in the reconstruction shown in figure 13 there is no significant shortening in central Chile prior to 20 Ma. We speculate that shortening started while the ridge was sweeping southward. In the time range 20-15 Ma, shortening in the northern part of the central segment at the latitude of La Serena might have been slightly higher than in the south at the latitude of Santiago. Since 15 Ma, the ridge has been subducting continuously under the central segment of the Andes with an estimated 100 km of shortening. Since shortening strongly decreases southward, this resulted in about 15° clockwise rotation of the southern segment.

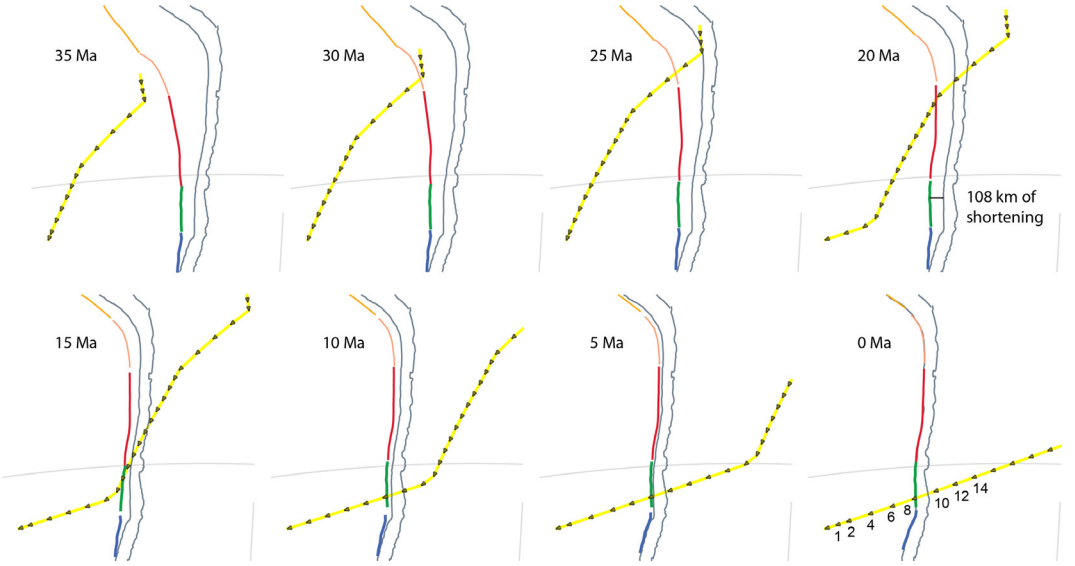

FIG. 13. Conceptual model for the origin of the Maipo Orocline. Evolution of the Juan Fernández Ridge (JFR) since 35 Ma (reconstruction of the subduction of the expected Juan Fernández ridge using plate rotations as Yáñez *et al.* (2001)). The shape of the trench has been reconstructed according to the restoration of the Andean margin from Arriagada *et al.* (2008). Between 35 and 25 Ma the JFR with a speculated oceanic plateau (Martinod *et al*., 2010) is subducted below the Central Andes with the initiation of the Bolivian Orocline. Between 22 and 12 Ma the JFR shows a rapid southward migration. From 12 Ma the JFR has migrated at a slower rate. The green segment of the margin record a slight clockwise rotation that is cancelled by a following slight counterclockwise rotation. The blue segment of the margin south of the JFR records a clockwise rotation.

Acknowledgements

Funding for this study was provided by Fondecyt-Chile (grants 1070964 and 1080468), Fondecyt grant PBCT Anillo ACT 18 and a cooperative program IRD/ Departamento de Geología, Universidad de Chile. Discussions and comments on earlier vesions of the manuscript by C. Mpodozis, R. Charrier, M. Farías, G. Yáñez and reviews by A. Rapalini, M. Calvo and J. Skarmeta greatly improved the original version of this article.

References

Arriagada, C.; Roperch, P.; Mpodozis, C.; Cobbold, P.R. 2008. Paleogene building of the Bolivian Orocline: Tectonic restoration of the central Andes in 2-D map view. Tectonics 27 (TC6014). doi: 10.1029/2008TC002269.

Astudillo, N.; Roperch, P.; Townley, B.; Arriagada, C.; Chauvin, A. 2009. Magnetic polarity zonation within the El Teniente copper-molybdenum porphyry deposit, central Chile. Mineralium Deposita 45 (1): 23-41. doi: 10.1007/s00126-009-0256-0.

Barazangi, M.; Isacks, B. 1976. Spatial distribution of earthquakes and subduction of the Nazca plate beneath South America. Geology 4: 686-692.

Beck, M.; Drake, R.; Butler, R. 1986. Paleomagnetism of Cretaceous volcanic rocks from central Chile and implications for the tectonics of the Andes. Geology 14: 132-136.

Beck, M.; Burmester, R.F.; García, A.; Rivano, S. 1990. Paleomagnetic results from Cretaceous rocks in the Llaillay-San Felipe-Putaendo region: implications for block rotations in the Andean forearc. Revista Geológica de Chile 17 (2): 115-130.

Besse, J.; Courtillot, V. 2002. Apparent and true polar wander and the geometry of the Geomagnetic Field over the last 200 Myr. Journal of Geophy-sical Research 107 (B11): EPM 6-1-EPM 6-31. doi: 10.1029/2000JB000050.

Carey, S.W. 1955. The orocline concept in geotectonics. Royal Society of Tasmania Papers and Proceedings 89: 255-288.

Charrier, R.; Wyss, A.R.; Flynn, J.J.; Swisher, C.C.; Norell, M.A.; Zapatta, F.; McKenna, M.C.; Novaceck, M.J. 1996. New evidence for late Mesozoic-early Cenozoic evolution of the Chilean Andes in the upper Tinguiririca valley (35°S), central Chile. Journal of South American Earth Sciences 9: 1-30.

Creixell, C.; Parada, M.A.; Roperch, P.; Morata, D.; Arriagada, C.; Pérez de Arce, C. 2006. Syntectonic

emplacement of the Middle Jurassic Concón Mafic Dike Swarm, Coastal Range, central Chile (33ºS). Tectonophysics 425: 101-122.

Demarest, H.H. 1983. Error analysis for the determination of tectonic rotation from paleomagnetic data. Journal of Geophysical Research 88: 4321-4328.

Farías, M.; Charrier, R.; Carretier, S.; Martinod, J.; Fock, A.; Campbell, D.; Cáceres, J.; Comte, D. 2008. Late Miocene high and rapid surface uplift and its erosional response in the Andes of Central Chile (33°-35°S). Tectonics 27 (TC1005). doi: 10.1029/2006TC002046.

Ferrando, R.; Roperch, P.; Morata, D.; Arriagada, C.; Ruffet, G.; Córdova, M. In press. A paleomagnetic and magnetic fabric study of the Illapel Plutonic Complex, Coastal Range, central Chile: Implications for emplacement mechanism and regional tectonic evolution during the Mid-Cretaceous. Journal of South American Earth Sciences.

Goguitchaichvili, A.; Chauvin, A.; Roperch, P.; Prevot, M.; Aguirre, L.; Vergara, M. 2000. Paleomagnetic results from the Miocene Farellones formation: a possible highest paleosecular variation during the Miocene. Geophysical Journal International 140: 357-373.

Gordon, R.G.; Jurdy, D.M. 1986. Cenozoic global plate motions. Journal of Geophysical Research 91: 2389-2406.

Hervé, F.; Munizaga, F.; Parada, M.A.; Brook, M.; Pankhurst, R.J.; Snelling, N.J.; Drake, R. 1988. Granitoids of the Coast Range of central Chile: geochronology and geologic setting. Journal of South American Earth Sciences 1: 185-194.

Irwin, J.; Sharp, R.; Spangler, R.; Drake, R. 1987. Some paleomagnetic constraints on the tectonic evolution of the Coastal Cordillera of central Chile. Journal of Geophysical Research 92: 3603-3614.

Isacks, B. 1988. Uplift of the Central Andes Plateau, and the bending of the Bolivian orocline. Journal of Geophysical Research 93: 3211-3231.

Kirschvink, J.L. 1980. The least-squares line and plane and the analysis of paleomagnetic data. Geophysical Journal of Royal Astronomical Society 62: 699-718.

Kurtz, A.; Kay, S.M.; Charrier, R.; Farrar, E. 1997. Geochronology of Miocene plutons and exhumation history of the El Teniente region, Central Chile (34°-35°S). Revista Geológica de Chile 24 (1): 75-90.

Le Roux, J.P.; Gómez, C.A.; Olivares, D.M.; Middleton, H. 2005. Determing the Neogene behavior of the Nazca plate by geohistory analysis. Geology 33 (3): 165-168.

Martinod, J.; Husson, L.; Roperch, P.; Guillaume, B.; Espurt, N. 2010. Horizontal subduction zones, convergence velocity and the building of the Andes. Earth and Planetary Sciece Letters 300 (3-4): 299-309.

McFadden, P.L.; McElhinny, M.W. 1988. The combined analysis of remagnetization circles and direct observations in paleomagnetism. Earth and Planetary Science Letters 87: 161-172.

Melnick, D.; Bookhagen, B.; Strecker, M.R.; Echtler, H.P. 2009. Segmentation of megathrust rupture zones from fore-arc deformation patterns over hundreds to millions of years, Arauco peninsula, Chile. Journal of Geophysical Research 114 (B01407). doi: 10.1029/2008JB005788.

Morata, D.; Féraud, G.; Schärer, U.; Aguirre, L.; Belmar, M.; Cosca, M. 2006. A new geochronological framework for Lower Cretaceous magmatism in the Coastal Range of central Chile. *In* Congreso Geológico Chileno, No. 11, 2: 509-512, Antofagasta.

Paquereau, P.; Fornari, M.; Roperch, P.; Thouret, J.C.; Macedo, O. 2008. Paleomagnetism, magnetic fabric, and $^{40}Ar/^{39}Ar$ dating of Pliocene and Quaternary ignimbrites in the Arequipa area, southern Peru. Bulletin of Volcanology 70: 977-997. doi:10.1007/s00445-007-0181-y.

Parada, M.A.; Nyström, J.O.; Levi, B. 1999. Multiple sources for the Coastal Batholith of central Chile (31-34ºS): geochemical and Sr-Nd isotopic evidence and tectonic implications. Lithos 46: 505-521.

Parada, M.A.; Feraud, G.; Fuentes, F.; Aguirre, L.; Morata, D.; Larrondo, P. 2005. Ages and cooling history of the Early Cretaceous Caleu pluton: testimony of a switch from a rifted to a compressional continental margin in central Chile. Journal of the Geological Society 162: 273-287.

Pineda, G.; Emparan, C. 2006. Geología del área Vicuña-Pichasca, Región de Coquimbo. Servicio Nacional de Geología y Minería, Carta Geológica de Chile, Serie Geología Básica, No. 97: 29 p. 1 mapa escala 1: 100.000.

Ramos, V.A.; Cristallini, E.; Pérez, O.J. 2002. The Pampean Oat·slab of lhe Central Andes. Journal of South American Earth Sciences 15 (1): 59-78.

Rivano, S.; Sepúlveda, P.; Hervé, M.; Puig, A. 1985. Geocronología K-Ar de las rocas intrusivas entre los 31º-32º latitud sur, Chile. Revista Geológica de Chile 24 (1): 63-74.

Vergara, M.; Levi, B.; Nyström, J.O. 1995. Jurassic and Early Cretaceous island arc volcanism, extension and subsidence in the Coast Range of central Chile. Geological Society of America Bulletin 107 (12): 1427-1440.

Willner, A.P.; Hervé, F.; Massonne, H.J. 2000. Mineral chemistry and pressure-temperature evolution of two contrasting high-pressure-low-temperature belts in the Chonos Archipelago, Southern Chile. Journal of Petrology 41: 309-330.

Willner, A.P. 2005. Pressure-temperature evolution of a Late Palaeozoic paired metamorphic belt in North-Central Chile (34°-35°30'S). Journal of Petrology 46: 1805-1833.

Yáñez, G.; Ranero, C.; von Huene, R.; Díaz, J. 2001. Magnetic anomaly interpretation across the southern central Andes (32-34°S): The role of the Juan Fernández Ridge in the late Tertiary evolution of the margin. Journal of Geophysical Research 106: 6325-6347.

Yáñez, G.; Cembrano, J.; Pardo, M.; Ranero, C.; Sellés, D. 2002. The Challenger-Juan Fernández-Maipo major tectonic transition of the Nazca-Andean subduction system at 33-34°S: geodynamic evidence and implications. Journal of South American Earth Sciences 15: 23-38.

Zijderveld, J.D.A. 1967. A.C. demagnetization of rocks: Analysis of results, *In* Methods in Palaeomagnetism (Collinson, D.W.; Creer, K.M.; Runcorn, S.K.; editors). Elsevier: 254-286.

Manuscript received: May 31, 2012; revised/accepted: November 24, 2012; available online: March 12, 2013.